water

MDPI

Article

Strontium Isotopic Composition as Tracers for Identifying Groundwater Recharge Sources in the Choushui River Alluvial Plain, Western Taiwan

Hao-Wei Huang [1], Shiuh-Tsuen Huang [2], Ruo-Mei Wang [3], Wen-Fu Chen [4], Chuan-Hsiung Chung [1] and Chen-Feng You [1,*]

[1] Department of Earth Sciences, National Cheng Kung University, Tainan 701, Taiwan; z11209078@ncku.edu.tw (H.-W.H.); bear_chung@mail.ncku.edu.tw (C.-H.C.)
[2] Department of Science Education and Application, National Taichung University of Education, Taichung 40306, Taiwan; hstsuen@mail.ntcu.edu.tw
[3] Institute of Earth Sciences, Academia Sinica, Taipei 115, Taiwan; rmwang4112@gmail.com
[4] Department of Tourism Management, Chia Nan University of Pharmacy and Science, Tainan 71710, Taiwan
* Correspondence: cfy20@mail.ncku.edu.tw

Abstract: Groundwater is a vital resource in the Chuoshui River alluvial plain (CSAP), a key agricultural area in Taiwan. Understanding groundwater recharge is crucial for sustainable water management amidst changing climatic conditions and increasing water demand. This study investigates the major ion composition, solute Sr concentrations, and $^{87}Sr/^{86}Sr$ ratios in groundwater and stream water from the Choushui River (CSR) to trace groundwater recharge sources. The Piper diagram reveals that most groundwater samples are of the freshwater Ca–HCO_3 type, aligning with the total dissolved solids (TDS) classification. TDS and major ion compositions indicate that groundwater near Baguashan Terrace (BGT) and Douliu Hill (DLH) primarily derives from stream water and rainwater. Na^+ and Cl^- enrichment in some aquifers of BGT and DLH is attributed to the dissolution of paleo-sea salt and mixing with paleo-seawater from sedimentary porewater. Elevated dissolved Sr concentrations and lower $^{87}Sr/^{86}Sr$ ratios in these aquifers further support the intrusion of paleo-seawater. Groundwater in the proximal fan shows high TDS due to intensive weathering, complicating the use of TDS as a tracer. Sr isotopic compositions and solute Sr^{2+} concentrations effectively distinguish recharge sources, revealing that the CSR mainstream primarily recharges the proximal fan and BGT region, while CSR tributaries and rainwater mainly recharge the DLH region. This study concludes that Sr isotopic compositions and solute Sr^{2+} concentrations are more reliable than TDS and major ion compositions in identifying groundwater recharge sources, enhancing our understanding of groundwater origins and the processes affecting water quality.

Keywords: $^{87}Sr/^{86}Sr$; groundwater recharge; Choushui River Alluvial Plain

check for updates

Citation: Huang, H.-W.; Huang, S.-T.; Wang, R.-M.; Chen, W.-F.; Chung, C.-H.; You, C.-F. Strontium Isotopic Composition as Tracers for Identifying Groundwater Recharge Sources in the Choushui River Alluvial Plain, Western Taiwan. *Water* **2024**, *16*, 2151. https://doi.org/10.3390/w16152151

Academic Editor: Umayadoss Saravana Kumar

Received: 18 June 2024
Revised: 24 July 2024
Accepted: 27 July 2024
Published: 30 July 2024

Copyright: © 2024 by the authors. Licensee MDPI, Basel, Switzerland. This article is an open access article distributed under the terms and conditions of the Creative Commons Attribution (CC BY) license (https://creativecommons.org/licenses/by/4.0/).

1. Introduction

Groundwater serves as the essential water resource in the Chuoshui River alluvial plain (CSAP), recognized as a critical groundwater reservoir and agricultural region in Taiwan. It is also among the earliest areas in Taiwan to have developed and utilized groundwater resources. The demand for groundwater has significantly increased due to rapid economic growth, industrial expansion, and population rise. However, groundwater is not an infinite resource; its sustainability depends on renewal through groundwater recharge, which involves processes that replenish groundwater resources. Groundwater recharge is therefore crucial for water resource sustainability and the resilience of the water supply amidst changing climatic conditions and water demands [1,2]. Sustainable groundwater planning and management necessitate a quantitative description of the recharge process, including total volume, location, and residence time [3]. More and more studies have discussed the relationship between groundwater recharge variability and climate change [4–7],

highlighting the importance of clarifying groundwater recharging sources. Investigations into groundwater recharge sources will aid in future applications to explore the impacts of climate change and water resource management.

$^{87}Sr/^{86}Sr$ ratios are valuable tracers for identifying fluid sources and migration pathways in natural settings. Both ^{87}Sr and ^{86}Sr are stable isotopes, part of ^{87}Sr can be produced through the radioactive decay of ^{87}Rb, so-called radiogenic ^{87}Sr. The variations in the variations in $^{87}Sr/^{86}Sr$ ratios within minerals are predominantly influenced by the age and Rb content of the parent rocks. Therefore, older rocks typically exhibit higher $^{87}Sr/^{86}Sr$ ratios compared to younger rocks with the same initial Rb/Sr ratio. Over geological time, rocks of a certain age that are rich in minerals with high Rb/Sr ratios (such as granites in the continental crust) will develop a higher $^{87}Sr/^{86}Sr$ ratio than those with lower Rb/Sr ratios (like oceanic basalt). It is widely accepted that Sr isotopes are not fractionated by biological processes or low-temperature abiotic chemical reactions (e.g., mineral dissolution and precipitation) [8,9]. Consequently, the $^{87}Sr/^{86}Sr$ ratio in waters is predominantly governed by the chemical weathering of regional materials. Sr concentrations may change due to processes such as evaporation or mixing of waters from different sources, but without causing the fractionation of the $^{87}Sr/^{86}Sr$ ratio. Thus, variations in the $^{87}Sr/^{86}Sr$ ratio can be used as a proxy to trace strontium from different origins [10–12]. For instance, rainwater usually exhibits an average $^{87}Sr/^{86}Sr$ value of 0.712, while seawater has an average $^{87}Sr/^{86}Sr$ value of 0.709. The $^{87}Sr/^{86}Sr$ ratios of river water from silicate sources are typically more likely to be radiogenic ratios (could be up to ~0.720) than those of carbonate sources [8,13,14]. Sr isotopes have been widely employed to identify the different sources of groundwater recharge and establish mass-balance calculations to assess recharge rates [11,13–16].

Here, we compare the $^{87}Sr/^{86}Sr$ compositions and solute Sr levels of stream water from the Choushui River (CSR) and regional rainwater with groundwater samples in the recharging area to evaluate the relative contribution of CSR's stream water and rainwater to the local aquifer. Total dissolved solid (TDS) and major components are used to discern the influence of weathering processes and source mixing and to examine these factors as tracers of groundwater sources in this study area. The main objectives of this study are as follows: (1) assess whether the Sr isotopic composition and major ion chemistry of groundwater can be used as proxies to trace groundwater recharge in CSAP; (2) identify the recharge sources of different aquifers.

2. Study Area

The CSAP is situated in Changhua and Yunlin Counties, in western central Taiwan. The CSR, Taiwan's longest river, boasts an alluvial fan spanning approximately 2431 km^2, characterized by elevations below 100 m. Its eastern boundary is outlined by the Baguashan Terrace (BGT) and Douliu Hill (DLH) of the Western Foothills, while the Taiwan Strait delineates its western boundary (Figure 1). To the north and south, the Wu and Beigang rivers serve as the defining boundaries, respectively. The unconsolidated sediments underlying the alluvial fan are of late Quaternary age, with grain size decreasing from the proximal to distal fan [17,18]. CSAP has experienced four cycles of marine transgression–regression in this area, which can be roughly divided into four overlapping sequences comprising four marine sequences and four non-marine sequences [17–19]. Generally, the formation of non-marine sequences, consisting of coarse sediment sizes ranging from medium sand to gravel and exhibiting high permeability, can be considered aquifers. In contrast, formations of marine sequences, characterized by fine sediment sizes ranging from clay to fine sand, exhibiting low-permeability, can be considered aquitards (Figure 2). The hydrogeological formation of the upper region is Toukoshan Formation, which is Quaternary molasse sediments of conglomerate and sand or sandstone and is regarded as an unconfined aquifer and an important groundwater recharge area (Figure 2) [17,19,20]. The catchment of CSR's mainstream and tributaries also covers the Kueichulin Formation and Cholan Formation. Kueichulin Formation comprises thick, light grey sandstones interbedded with grey mud-

stones, interpreted as shoreface deposits. The Cholan Formation is composed of very fine–fine-grained sandstones intercalated with grey mudstones [17,19].

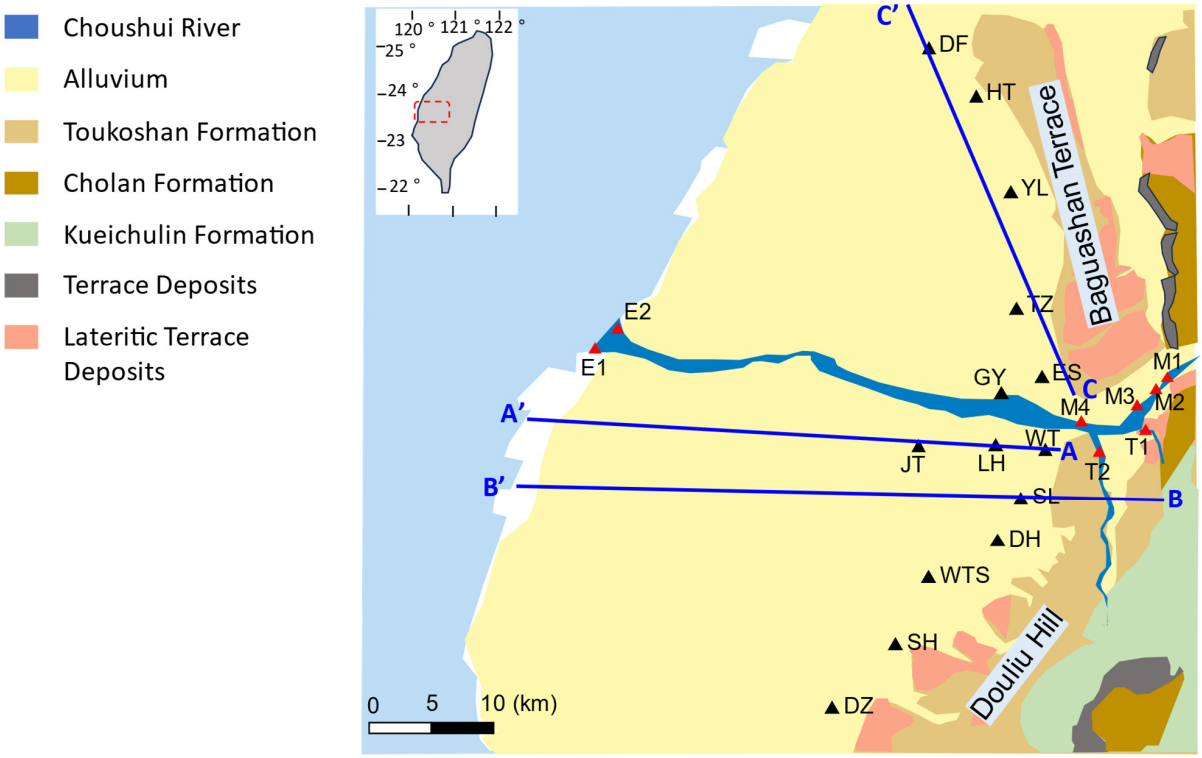

Figure 1. The sample sites and geological map of Choshui River Alluvial Plain (M—mainstream of CSR; T—tributaries of CSR; E—estuary of CSR; YL—Yuanlin well; HT—Huatan well; DF—Dungfang well; SL—Shiliu well; DH—Donghe well; WTS—Wentsu well; DZ—Dongzong well; SH—Sanhe well; GY—Ganyuan well; ES—Ershui well; TZ—Tianzhong well; JT—Jington well; LH—Liuhe well; WT—Wutu well).

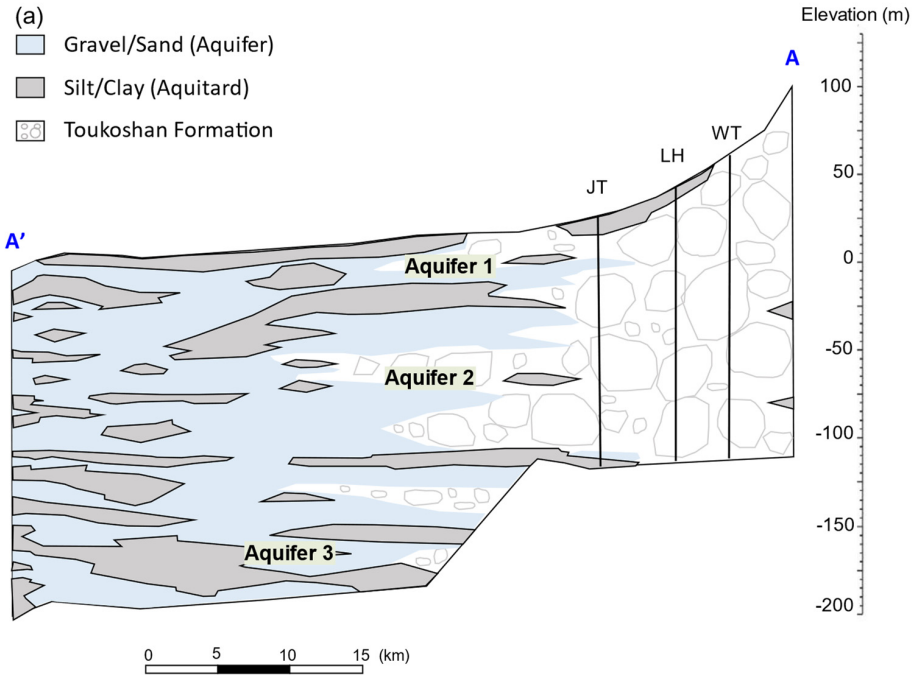

Figure 2. *Cont.*

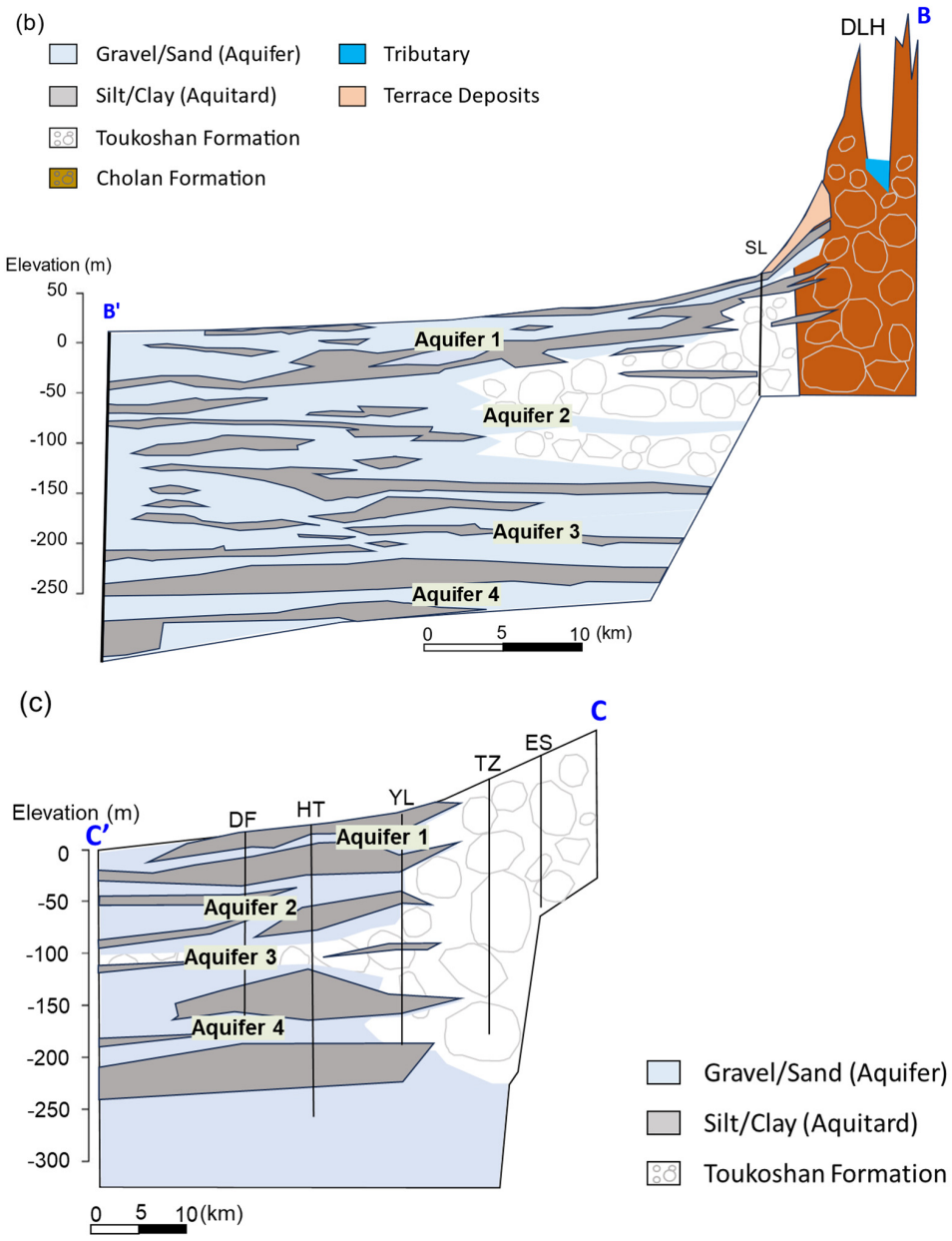

Figure 2. The (**a**) A–A′, (**b**) B–B′, and (**c**) C–C′ profiles illustrate the hydrogeological characteristics of the CSAP (adapted from [17,19]).

3. Materials and Methods

A total of 8 water samples were collected along the mainstream, tributaries, and estuaries of the CSR in August and September 2002. Samples from the mainstream and tributaries located near the upper reaches of the CSAP. A total of 31 groundwater samples were collected from the monitoring well in different aquifer near BGT, DLH, and proximal fan in April and July 2003. A regional geological map showing all the sampling sites is presented in Figure 1. All water samples were stored in acid-cleaned PP bottles and were filtered through a 0.45 µm Whatman nylon syringe filters. Then, water samples were acidified by HNO_3 and stored at 4 °C until analysis.

All the major elements, Sr^{2+} concentration, and $^{87}Sr/^{86}Sr$ ratio were measured in the Isotope Geochemistry Lab at the National Cheng Kung University, Taiwan. Major anions of Cl^-, SO_4^{2-}, and NO_3^- were determined using Alltech ion chromatography (IC) with an average precision of 5%. Major cations and solute Sr contents were measured by an inductively coupled plasma mass spectrometer (ICP-MS, Thermo Finnigan Element 2,

Thermo Scientific, Waltham, MA, USA) with an average analytical precision of 2%. HCO_3^- concentrations were calculated by charge balance.

For Sr purification, water samples were first converted to the nitric acid form using 3 N HNO_3 and then evaporated to precipitate all dissolved salts. The precipitates were subsequently redissolved in 1 N HNO_3 for further purification. Eichrom Sr^{SPEC} resin (bed volume 0.5 mL), pre-conditioned with 3 N HNO_3, was packed into acid-cleaned ion-exchange columns. Samples were loaded onto the columns and eluted with 8 mL of 3 N HNO_3 to remove additional isobaric interference elements such as Zr and Rb. The purified Sr samples were then eluted with 4 mL of Milli-Q water. The eluted solutions were evaporated to dryness and then redissolved in 2 µL of 0.25 N distilled HCl before being loaded onto a Ta filament. Strontium isotopic compositions were determined using a Finnigan thermal ionization mass spectrometer (TIMS, Triton, TI, USA), equipped with 9 Faraday cups and a secondary electron multiplier. The measured $^{87}Sr/^{86}Sr$ ratio was normalized to measured $^{88}Sr/^{86}Sr$ ratios of 8.37521 for potential mass fractionation correction. Instrumental performance was monitored by long-term measurements of NIST SRM987 (0.710247 ± 0.000005, n = 61) [21].

4. Results

4.1. Major Element Composition

Measured major element and Sr concentrations, as well as strontium isotopic ratios, in the collected river and groundwater samples are presented in Table 1. In CSR's mainstream samples, Ca^{2+} (1.67–1.94 mM) and Mg^{2+} (0.61–0.63 mM) are the predominant cations, constituting 65–67 Eq% and 22–24 Eq% of the cationic charge, respectively. Na^+ and K^+ account for 10 Eq% and 1 Eq%. The anionic charge is primarily from SO_4^{2-} (1.42–1.54 mM, 53–59 Eq%) and HCO_3^- (2.01–2.51 mM, 39–43 Eq%) (Table 1). In tributary samples, Ca^{2+} (0.97–1.06 mM) and Mg^{2+} (0.32–0.44 mM) represent 57–62 Eq% and 20–24 Eq% of the cationic charge, while Na^+ and K^+ account for 16–17 Eq% and 2 Eq%. Anionic charge is mainly from SO_4^{2-} (0.34–0.64 mM, 39–43 Eq%) and HCO_3^- (2.22–2.25 mM, 60–72 Eq%) (Table 1). Estuary samples show Na^+ and Cl^- are two dominant ions, accounting for 309–394 mM and 342–532 mM, respectively (Table 1).

Groundwater from the proximal fan shows similar major elemental compositions to CSR fresh river samples, with Ca^{2+} (1.83–4.00 mM) and Mg^{2+} (0.66–1.27 mM) making up 66–72 Eq% and 22–27 Eq% of the cationic charge. SO_4^{2-} (1.64–1.92 mM) and HCO_3^- (3.20–6.81 mM) account for 26–47 Eq% and 46–66 Eq% of the anionic charge (Table 1). In contrast, groundwater near BGT and DLH has higher Na^+ (12–47 Eq% of cationic charge) and HCO_3^- (53–97 Eq% of anionic charge) proportions (Table 1). The groundwater composition findings are similar to the findings of Chang et al. [22].

The total dissolved solids for CSR's mainstream and tributary are calculated from the sum of major ions, which range from 323 to 357 mg/L and 184 to 225 mg/L, while for those from near BGT, DLH, and proximal fan account for 157–283 mg/L, 140–447 mg/L, and 350–678 mg/L, respectively (Table 1). Based on the classification by [23], all samples belong to freshwater.

Table 1. Major ion composition and Sr isotopic composition of CSR's stream water and groundwater in CSAP.

Sample ID	Sample Type	Elevation (m)	Temperature (°C)	pH	Na^+ (mmol/L)	K^+ (mmol/L)	Mg^{2+} (mmol/L)	Ca^{2+} (mmol/L)	Sr^{2+} (μmol/L)	Cl^- (mmol/L)	NO_3^- (mmol/L)	SO_4^{2-} (mmol/L)	TDS (mg/L)	$^{87}Sr/^{86}Sr$	HCO_3^- (mmol/L)	Water Type
Choushui River																
CSR-M1	Mainstream	N.A.	N.A.	N.A.	0.540	0.066	0.630	1.740	4.080	0.056	0.051	1.490	330	0.714054	2.259	mixing type
CSR-M2	Mainstream	N.A.	N.A.	N.A.	0.540	0.064	0.610	1.690	4.023	0.054	0.059	1.420	323	0.714007	2.251	mixing type
CSR-M3	Mainstream	N.A.	N.A.	N.A.	0.530	0.062	0.620	1.670	4.136	0.045	0.059	1.530	325	0.713830	2.008	mixing type
CSR-M4	Mainstream	N.A.	N.A.	N.A.	0.570	0.074	0.630	1.940	3.977	0.071	0.117	1.540	357	0.713986	2.516	mixing type
CSR-T1	Tributary	N.A.	N.A.	N.A.	0.510	0.057	0.320	0.970	1.886	0.054	0.160	0.340	184	0.710263	2.253	$Ca\text{-}HCO_3$
CSR-T2	Tributary	N.A.	N.A.	N.A.	0.640	0.061	0.440	1.060	2.614	0.048	0.150	0.640	225	0.710535	2.223	$Ca\text{-}HCO_3$
CSR-E1	Estuary	N.A.	N.A.	N.A.	309	3.3	19.2	6.7	43.352	342	N.A.	19.3	N.A.	0.709988	N.A.	
CSR-E2	Estuary	N.A.	N.A.	N.A.	397	6.8	41.9	9.6	57.909	532	N.A.	28.3	N.A.	0.709348	N.A.	
near Baguashan Terrace																
YL-F1	Groundwater	−45	24	7.54	0.639	N.D.	0.329	0.808	1.262	0.210	N.D.	N.D.	190	0.713010	2.703	$Ca\text{-}HCO_3$
YL-F3-1	Groundwater	−75	23.8	7.59	0.778	N.D.	0.354	0.630	0.843	0.310	N.D.	N.D.	171	0.713277	2.437	$Ca\text{-}HCO_3$
YL-F3-2	Groundwater	−110	24.5	7.85	0.961	N.D.	0.385	1.258	1.196	0.338	N.D.	0.030	233	0.712864	3.847	$Ca\text{-}HCO_3$
YL-F4	Groundwater	−160	24.2	7.96	1.130	0.020	0.354	1.058	1.309	0.310	N.D.	N.D.	216	0.713024	3.664	$Ca\text{-}HCO_3$
HT-F1	Groundwater	5	25.2	7.36	1.991	0.120	1.221	3.250	3.814	4.423	N.D.	0.486	754	0.712929	5.658	$Ca\text{-}HCO_3$
HT-F2	Groundwater	−45	24.5	6.95	1.530	0.070	0.258	0.275	0.483	0.479	0.008	0.243	249	0.712589	1.694	mixing type
HT-F3	Groundwater	−97	24.9	7.44	0.878	N.D.	0.208	0.475	0.530	0.250	N.D.	N.D.	157	0.712939	1.994	$Ca\text{-}HCO_3$
HT-F4	Groundwater	−252	25.6	8.02	1.670	0.030	0.360	1.333	1.402	0.558	N.D.	N.D.	283	0.713383	4.526	$Ca\text{-}HCO_3$
DF-F3	Groundwater	−98	24.9	7.63	1.439	0.020	0.278	0.783	0.969	0.338	0.003	N.D.	208	0.713491	3.240	$Ca\text{-}HCO_3$
DF-F4	Groundwater	−172	25.2	7.94	1.539	0.020	0.278	1.158	1.316	0.451	0.002	N.D.	256	0.713413	3.978	$Ca\text{-}HCO_3$
near Douliu Hill																
SL-F1	Groundwater	52	25	6.44	0.639	0.010	0.479	0.525	0.947	0.250	0.002	0.502	188	0.713355	1.403	$Ca\text{-}HCO_3$
SL-F2	Groundwater	−15	24.9	6.92	0.722	0.020	0.380	0.803	0.365	0.369	0.003	0.139	180	0.712699	2.457	$Ca\text{-}HCO_3$
DH-F1	Groundwater	−7	24.6	6.95	0.739	N.D.	0.613	0.933	1.096	0.338	N.D.	0.650	248	0.712173	2.190	$Ca\text{-}HCO_3$
DH-F2	Groundwater	−165	24.6	7.15	0.570	0.020	0.892	1.158	1.849	0.479	0.116	0.759	278	0.711573	2.574	$Ca\text{-}HCO_3$
WTS-F1	Groundwater	22	23.7	6.96	0.791	0.020	0.633	1.728	1.918	0.389	0.004	0.745	349	0.711540	3.651	$Ca\text{-}HCO_3$
WTS-F2	Groundwater	−44	24.4	7.11	0.822	0.020	0.380	0.928	0.468	0.220	0.050	0.521	262	0.711577	2.144	$Ca\text{-}HCO_3$
SH-F1	Groundwater	49	24.8	7.11	1.491	0.058	0.658	1.228	2.237	0.710	0.004	0.034	274	0.711381	4.539	$Ca\text{-}HCO_3$
SH-F2	Groundwater	−15	25	7.25	1.335	0.030	0.278	0.803	0.799	0.200	0.003	N.D.	196	0.711245	3.323	$Ca\text{-}HCO_3$
DZ-F1	Groundwater	−7	28.5	7.55	1.730	0.027	0.228	0.828	0.811	0.110	0.002	N.D.	242	0.711401	3.756	$Ca\text{-}HCO_3$
DZ-F2	Groundwater	−138	27.5	7.96	1.117	0.018	0.127	0.903	1.884	0.170	0.003	N.D.	218	0.711020	3.021	$Ca\text{-}HCO_3$
DZ-F3	Groundwater	−179	27.9	7.86	1.652	0.120	0.808	1.880	2.831	0.997	0.066	0.943	447	0.711147	4.199	$Ca\text{-}HCO_3$
DZ-F4	Groundwater	−245	29.4	7.84	0.770	N.D.	0.157	0.375	1.963	0.170	N.D.	0.060	140	0.711450	1.545	$Ca\text{-}HCO_3$
proximal fan																
WT-F1	Groundwater	5	24.5	7.56	0.561	0.040	0.988	2.700	3.265	0.420	0.114	1.200	471	0.713220	6.810	$Ca\text{-}HCO_3$
ES-F1	Groundwater	−7	24.2	7.07	0.570	0.020	0.658	1.838	2.308	0.420	0.136	0.715	350	0.713600	3.201	$Ca\text{-}HCO_3$
GY-F1	Groundwater	33	24.3	7.35	0.561	0.060	1.267	4.000	4.932	0.420	0.077	1.923	678	0.713993	3.596	$Ca\text{-}HCO_3$
GY-F2	Groundwater	−25	23.9	7.72	0.439	0.040	0.963	2.305	1.119	0.451	0.073	1.644	475	0.713938	5.640	mixing type
JT-F1	Groundwater	10	26.3	7.58	0.709	0.070	1.192	3.550	4.064	0.451	0.002	1.675	603	0.713699	4.438	$Ca\text{-}HCO_3$
JT-F2	Groundwater	−66	24	7.64	0.570	0.040	0.833	2.575	3.505	0.338	0.020	1.127	480	0.713022	6.459	$Ca\text{-}HCO_3$
LH-F1	Groundwater	22	24.9	7.66	0.530	0.040	0.963	2.550	3.242	0.310	0.056	1.096	438	0.713600	4.813	$Ca\text{-}HCO_3$
LH-F1	Groundwater	−48	23.8	7.48	0.539	0.050	1.217	3.025	1.701	0.369	0.129	1.375	566	0.713039	5.037	$Ca\text{-}HCO_3$
TZ-F2	Groundwater	−70	23.9	7.57	0.600	0.040	1.013	3.125	4.060	0.250	0.109	1.458	533	0.714049	5.824	$Ca\text{-}HCO_3$
TZ-F4	Groundwater	−175	23.9	7.47	0.570	0.040	0.938	2.775	4.027	0.420	0.115	1.531	520	0.714082	5.043	$Ca\text{-}HCO_3$

Note(s): (N.D.—not detectable; N.A.—not available; M—mainstream; T—tributary; E—estuary; F—aquifer).

4.2. Piper Diagram

The Piper diagram illustrates three types of hydrochemical components (Figure 3): (1) Ca-HCO_3, (2) a mixing of Na-HCO_3 and Ca-HCO_3, and (3) a mixing of $CaCl_2$ and Ca-HCO_3 (Figure 3). Ca-HCO_3 type represents typical fresh groundwater and could result from water reacting with carbonates in the soil [24–26], which is primarily found in recharging areas. One sample from the vicinity of BGT is located on the evolutionary trend from Ca-HCO_3 to Na-HCO_3 type. Na-HCO_3 type is characterized by high Na^+ but low Cl^-. The cation exchange between Ca^{2+} in the Ca-HCO_3 type water and Na^+ in marine de-posits could generate an evolutionary trend. The marine-derived cations of Na^+, which is initially sorbed to the clay mineral surfaces when seawater interacts with sediments. Subsequently, when the aquifers are no longer immersed in seawater, the inflow of freshwater would flush through the saline deposits, resulting in the replacement of Ca^{2+} by the exchanger with concomitant release of Na^+. This feature ultimately results in a Na-HCO_3 water type groundwater, indicating a longer residence time of groundwater. (Figure 3) [24,27]. The sediment in CSAP is comprised of marine deposits with texture characterized by alternating coarse sand/gravel and fine silt/clay [28]. Therefore, the mixing type of Na-HCO_3 and Ca-HCO_3 could originate from the freshening process of saline deposit with fresh groundwater from the middle fan or CSR [24,27]. One groundwater sample from proximal fan and all CSR's mainstream samples belong to the mixing type between $CaCl_2$ and Ca-HCO_3. $CaCl_2$ water type typically indicates the transition of seawater intrusion which induces cation exchanging between the seawater and aquifer. Na^+ and Cl^- are the dominant ions in seawater. When seawater intrudes in a fresh aquifer, Na^+ would replace the Ca^{2+} and release the Ca^{2+} into groundwater. The water type transforms from Na-Cl type to $CaCl_2$ [22]. However, CSR's mainstream and the samples in the proximal fan are located in the recharging area. It is unlikely to suffer from seawater intrusion. Moreover, Cl concentration in the CSR's mainstream is around 0.05–0.07 mM, much lower than estuary and regional groundwater with average value of 0.56 mM and 0.11–0.99 mM, respectively (Table 1). In contrast, it is notable that SO_4^{2-} concentration in these samples are higher than in other regional groundwater and tributaries (Figure 3), suggesting that mixing water cannot be attributed to seawater intrusion. Dissolved sulphate probably comes from sulfide oxidation because pyrite is ubiquitous in this catchment, while there is no reported evaporite [29–31].

4.3. Solute Sr Concentration and Its Isotopic Composition

The samples of CSR's mainstream exhibit Sr concentration ranging from 3.977 to 4.136 μM, with $^{87}Sr/^{86}Sr$ ratios between 0.713830 and 0.714054. In comparison, CSR's tributaries have relatively lower $^{87}Sr/^{86}Sr$ ratios from 0.710263 to 0.710535 and Sr concentrations between 1.886 and 2.614 μM (Table 1). $^{87}Sr/^{86}Sr$ ratios in CSR's estuaries are lowest compared to those in the mainstream and tributaries, ranging from 0.709348 to 0.709988, with significantly enriched Sr concentrations between 43.352 and 57.909 μM (Table 1). Groundwater in the proximal fan shows Sr levels varying from 1.119 to 4.932 μM and $^{87}Sr/^{86}Sr$ ratios from 0.713022 to 0.714082. Groundwater near BGT displays a wide range of Sr concentrations, from 0.483 to 3.814 μM, and $^{87}Sr/^{86}Sr$ ratios between 0.712589 and 0.714082. Samples from the DLH area have Sr concentrations ranging from 0.468 to 2.831 μM and $^{87}Sr/^{86}Sr$ ratios from 0.711020 to 0.713355 (Table 1).

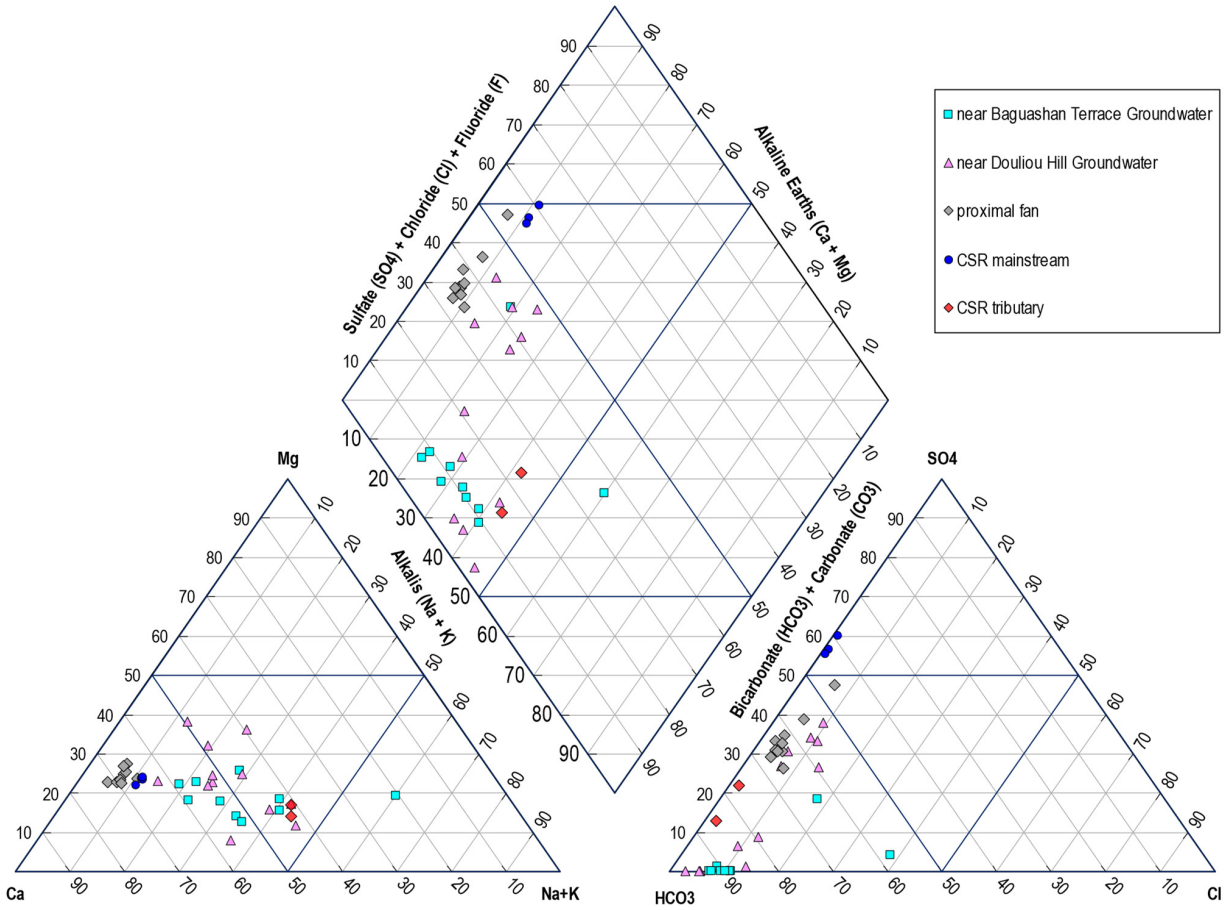

Figure 3. Piper diagram of water samples in this study.

5. Discussion

5.1. Evaluating TDS and Chloride as Tracers for Groundwater Source Identification

TDS can be used as a tracer since it differs from different water sources. For instance, fresh water, such as rainwater, exhibits lower TDS values than groundwater, as groundwater generally experiences more rock–water interaction. Some studies have employed stable isotope and electrical conductivity (EC) as natural tracers to identify water sources, fluid migration, and water mass mixing [32–35]. TDS in water is closely related to EC [36], suggesting TDS is also a potential tracer to determine the water source. Chloride ions are considered to originate from precipitation and cannot be lost through evapotranspiration in areas without evaporites. Therefore, chloride content is treated as a conservative element in groundwater, and chloride mass balance is used to trace water sources [34,37–40]. Therefore, we plot Cl^- vs. TDS diagrams to preliminarily differentiate groundwater sources and evaluate the effectiveness of these tracers.

The hydrogeological maps of the vicinity of sampling sites in the BGT area (Figure 1) show that rainwater and the main CSR are considered two potential recharge sources. As for the DLH region, we also include the impact of CSR's tributary, which flows through this region (Figure 1). The plot of Cl^- vs. TDS in groundwater near BGT and DLH region reflects that the TDS values of near-BGT groundwater fall between the CSR's mainstream and rainwater, except for the sample of HT-F1 and SH-F1 (Figures 4a and 5a), implying that the CSR's mainstream and rainwater are two important recharging sources. In the DLH region, some groundwater TDS values are close to those of the tributary, suggesting that the tributary, along with the CSR's mainstream and rainwater, is a likely input source (Figure 5a). In both regions, most groundwater samples exhibit high chloride concentrations than CSR and rainwater, limiting the use of chloride as groundwater tracers (Figure 5a). The

plot of Cl^- vs. TDS in proximal fan groundwater demonstrates that the TDS and chloride contents are all higher than CSR and rainwater. Therefore, the possible contribution of proximal fan groundwater cannot be determined by these indexes (Figure 6a).

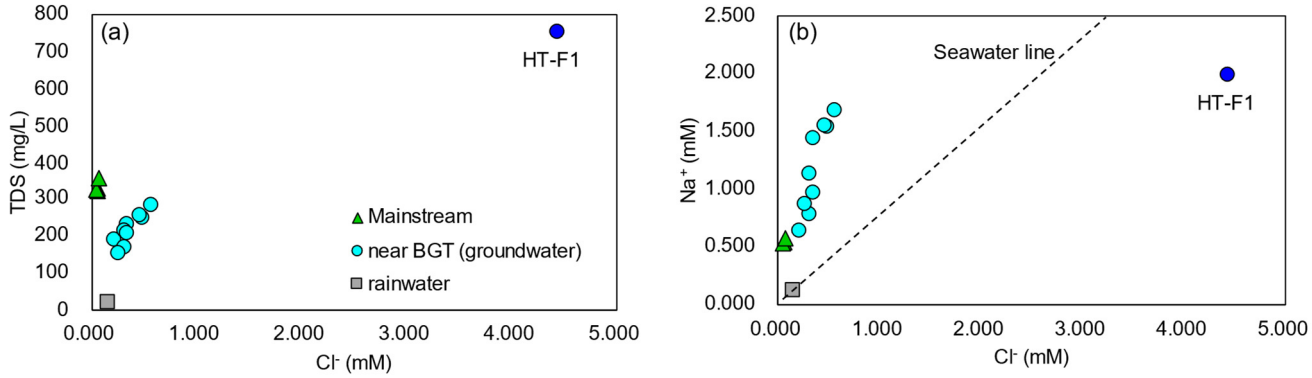

Figure 4. (**a**) TDS vs. Cl content and (**b**) Na^+ vs. Cl^- content for the groundwater collected from near the BGT region and stream water. The mean rainwater value quotes from Li et al. [41]. The seawater line shown in the dashed line reflects the Na/Cl ratio of seawater.

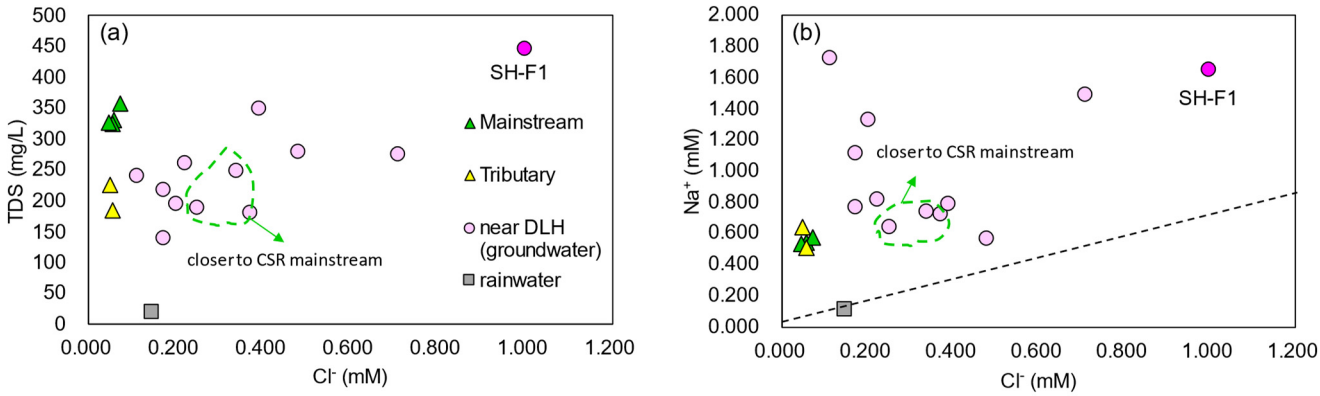

Figure 5. (**a**) TDS vs. Cl content and (**b**) Na^+ vs. Cl^- content for the groundwater collected from near-DLH region and stream water. The mean rainwater value quotes from Li et al. [41]. The seawater line shown in the dashed line reflects the Na/Cl ratio of seawater.

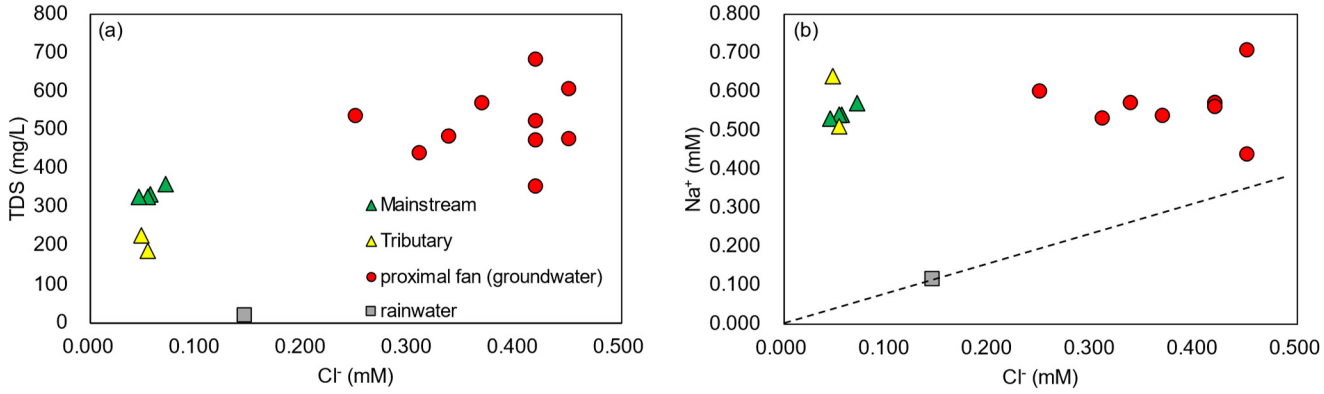

Figure 6. (**a**) TDS vs. Cl content and (**b**) Na^+ vs. Cl^- content for the groundwater collected from proximal fan and stream water. The mean rainwater value quotes from Li et al. [41]. The seawater line shown in the dashed line reflects the Na/Cl ratio of seawater.

5.2. Identifying Groundwater Recharging Sources through $^{87}Sr/^{86}Sr$ and 1/Sr

5.2.1. Groundwater in Proximal Fan

The mainstream and tributaries of CSR are two potential important contributors in the proximal fan. The plot of $^{87}Sr/^{86}Sr$ vs. 1/Sr clearly shows that proximal fan groundwater is predominantly influenced by inputs from CSR's mainstream (Figure 7). Wells situated closer to the CSR's mainstream demonstrate $^{87}Sr/^{86}Sr$ and Sr concentrations closely resembling those of river water. For example, stations of ES and TZ, which are the closest sites to the mainstream, exhibit $^{87}Sr/^{86}Sr$ ratios ranging from 0.713600 to 0.714082 and Sr values ranging from 2.31 μM to 4.06 μM, which are similar to the values of CSR's mainstream (Table 1). However, samples (LH-F2 and JT-F2) in the second aquifer of two wells, which are close to the tributary, show relatively lower $^{87}Sr/^{86}Sr$ (Figure 7 and Table 1). This finding suggests that these two aquifers may receive a small portion of contribution from tributaries. However, the relatively low $^{87}Sr/^{86}Sr$ ratios of some aquifers could also be influenced by carbonate weathering and rainwater mixing. The influence of carbonate weathering will be discussed in Section 5.5. While rainwater might also cause a decrease in the $^{87}Sr/^{86}Sr$ ratios, the element concentrations do not show dilution effects from rainwater infiltration (Figure 6 and Figure S3), with multiple element concentrations remain similar to those of river water. Therefore, compared to the carbonate weathering and rainwater mixing, the tributary contribution is more likely to induce the decrease in the $^{87}Sr/^{86}Sr$ ratios in LH-F2 and JT-F2 aquifers. Major ion composition of groundwater in the proximal fan influenced by weathering processes, limiting the use of TDS and major ion compositions as proxies for tracing water bodies. However, the $^{87}Sr/^{86}Sr$ ratios of groundwater clearly point out that the primary recharging sources in the proximal fan are CSR's mainstream.

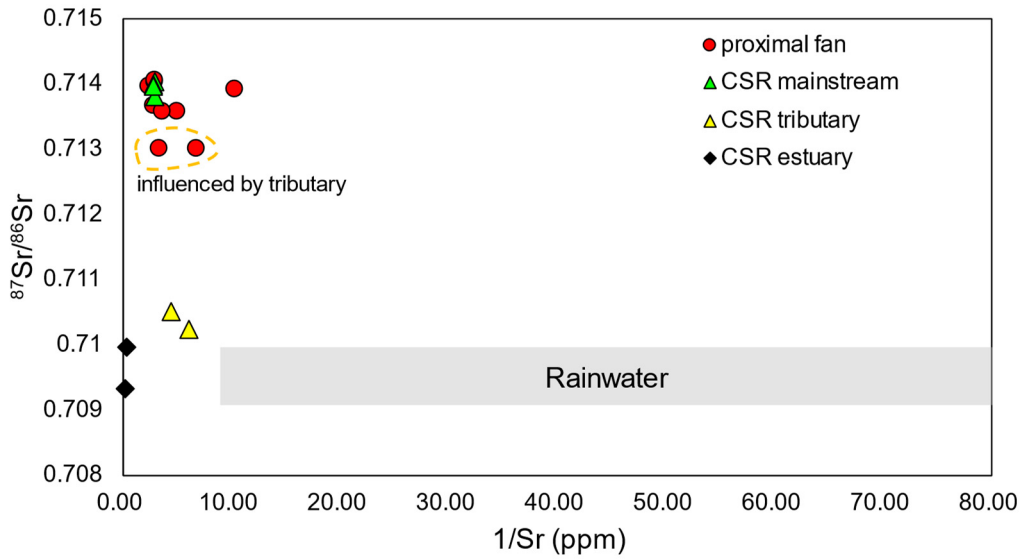

Figure 7. The 1/Sr vs. $^{87}Sr/^{86}Sr$ plot of proximal fan groundwater, CSR's stream water, and rainwater from Cheng et al. [42].

5.2.2. Groundwater near BGT and DLH

The results of major components reveal that most groundwater near BGT is influenced by rainwater and CSR's mainstream, with only one samples from the HT-F1 sites showing signs of paleo-seawater intrusion (Figure 4 and Figure S1). Therefore, we first compare the $^{87}Sr/^{86}Sr$ and 1/Sr ratios of CSR's mainstream, estuary, and rainwater. In the figure of $^{87}Sr/^{86}Sr$ and 1/Sr, the groundwater data of near BGT falls within the mixing region of rainwater and CSR's mainstream, indicating that these two sources are the primary contributors to the groundwater in this area (Figure 8). Moreover, the variations of major components are consistent with the results of Sr isotopic composition, suggesting that the groundwater near BGT is replenished by rainwater and CSR's mainstream.

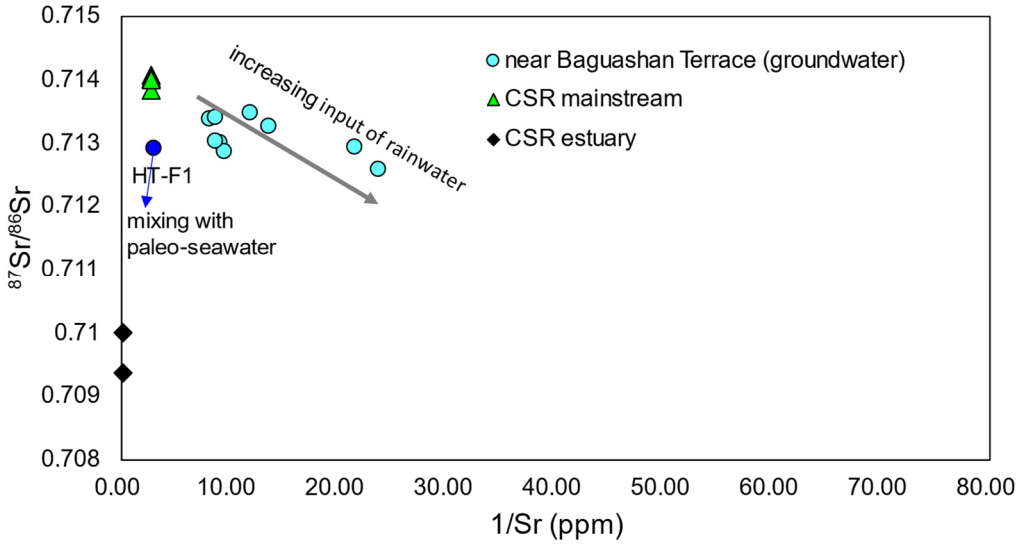

Figure 8. The 1/Sr vs. $^{87}Sr/^{86}Sr$ plot of near-BGT groundwater, CSR's stream water, and rainwater from Cheng et al. [42].

In addition to rainwater and the CSR's mainstream, the groundwater near DLH is also affected by the contributions of the CSR's tributaries. Similar to the groundwater near BGT, DLH wells (SL and DH), closer to the mainstream, exhibit more radiogenic $^{87}Sr/^{86}Sr$ ratios than the tributary (Figure 9 and Table 1). The $^{87}Sr/^{86}Sr$ ratios in other groundwater samples range between 0.711020 and 0.711577, approaching the $^{87}Sr/^{86}Sr$ values of the tributaries, supporting our assumption that the tributary is an essential source of near-DLH groundwater. In this region, aquifers with higher TDS and Cl concentrations exhibit elevated solute Sr concentrations (Table 1), indicating prolonged water–rock interaction. Stratigraphic profiles demonstrate that the first aquifer in this area is relatively thin (Figure 2b), which likely results in poor lateral connection, making it difficult for the aquifer to receive inputs from rainwater and CSR's stream water. Consequently, aquifers with low Sr concentrations suggest better lateral connection, a higher replenishment rate, and a greater susceptibility to rainwater infiltration. Therefore, low dissolved Sr concentrations in some aquifers indicate the dilution effect of rainwater (Figure 9).

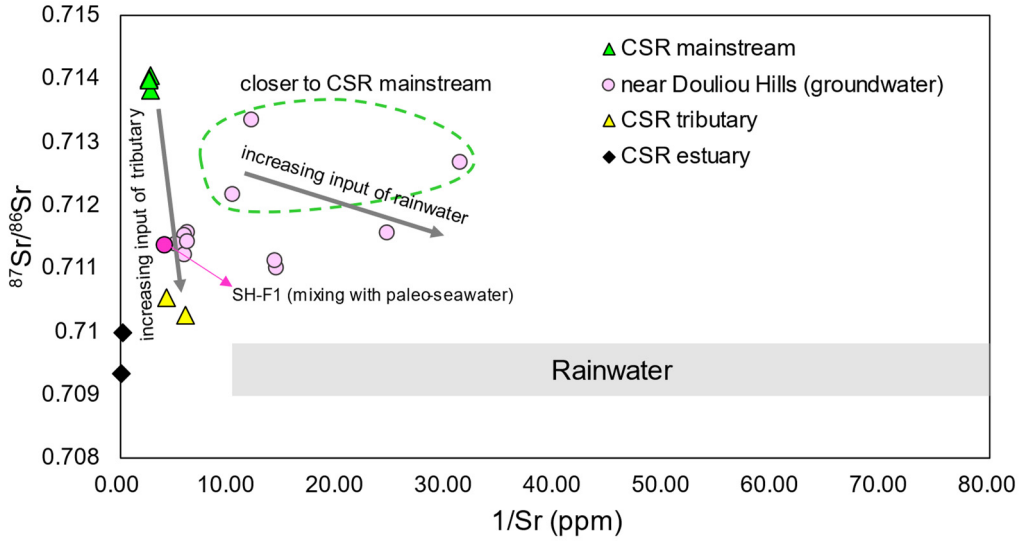

Figure 9. The 1/Sr vs. $^{87}Sr/^{86}Sr$ plot of near-DLH groundwater, CSR's stream water, and rainwater from Cheng et al. [42].

The contribution of rainwater cannot be excluded, as the δD and $\delta^{18}O$ composition of groundwater from the near-DLH region indicates that precipitation can contribute up to 50% to the groundwater recharge [35]. Although the $^{87}Sr/^{86}Sr$ ratio can indicate the characteristics of different water bodies, solute Sr levels would be influenced by rainwater dilution. Additionally, the Sr concentration in rainwater varies significantly, hindering the combination of 1/Sr with Sr isotopic composition as an indicator to differentiate water sources. Many studies use Cl^- to correct for the dilution effect caused by rainwater. However, it is based on the assumption that Cl^- originates only from precipitation. Sediments in the CSAP have undergone four instances of marine transgression, indicating that chloride sources are not limited to rainfall but also include paleo-sea salt. The high Na^+ and Cl^- characteristics of groundwater suggest potential contamination from paleo-sea salt dissolution, making Cl^- unsuitable for eliminating the dilution effect of rainwater. Therefore, further studies would benefit from using multi-isotopic systems ($^{87}Sr/^{86}Sr$ and stable water isotopes) to accurately estimate the contributions of various water sources and significantly enhance the ability to quantify the source contributions in various environments.

5.3. The Cause of High-Chloride and -Sodium Groundwater

Near-BGT and partial-DLH groundwater samples show higher chloride contents than the CSR's mainstream and rainwater, suggesting an additional endmember with high Cl^- concentrations. Chloride from anthropogenic inputs, such as domestic sewage or fertilizers, can be ruled out due to the lack of elevated NO_3^- and K^+ concentrations that are normally found in sewage and agricultural seepage (Table 1) [43]. The chloride ion source of deep groundwater may originate from the dissolution of paleo-sea salt or silicate weathering [44,45]. Since the uppermost aquitard was formed during marine transgression, the underlying aquifer was likely to be immersed in seawater as well. Therefore, paleo-sea salt may serve be dominant contributor to sodium and chloride ions in the groundwater. Silicate weathering is excluded. Su et al. [46] report that the average $^{87}Sr/^{86}Sr$ ratio in the silicate fraction of CSR's sediment is as high as 0.7200. If the Na^+ content in the groundwater originated from silicate weathering, the $^{87}Sr/^{86}Sr$ of groundwater should increase due to inputs from silicate weathering [14]. However, $^{87}Sr/^{86}Sr$ ratios of the near-BGT and -DLH groundwater do not show more radiogenic values (Figure 8).

Na^+ enrichment is evident in most wells, with Na concentrations exceeding the seawater line, suggesting an additional Na^+ source similar to that in BGT groundwater. Except for SH-F1, the Na-enriched groundwaters are likely involved in the freshening process of saline deposits similar to the phenomenon found in BGT groundwater, as Na^+ is the only cation that surpassed the Na^+ concentration of CSR's stream water in all samples (Figure 5b). This indicates that the chemistry of groundwater may not solely be affected by sea salt dissolution but also by an additional source of sodium (Figure 4b). Silicate weathering is a potential Na^+ source. However, silicate weathering is ruled out because $^{87}Sr/^{86}Sr$ ratios of the near-BGT and -DLH groundwater do not show more radiogenic values (Figure 8). This inference is also supported by the relationships between major components and Cl^-. Except for HCO_3^-, the concentrations of other major components (such as Mg^{2+}, Ca^{2+}, K^+, and SO_4^{2-}) in BGT groundwater, which are typically enriched by weathering processes, are not higher than those in river water. This suggests that the groundwater has not been affected by intensive silicate weathering as in a river system or long-term weathering process (Figure S1). Therefore, the source of Na^+ in the deep groundwater is more likely from the freshening process of saline deposit, where Na^+ is replaced by dissolved Ca in the freshwater and released into the groundwater.

5.4. Evidence of Paleo-Seawater Retention in Shallow Aquifers near BGT and DLH

The highest Cl^- in near-BGT and -DLH groundwater occurs in the shallowest aquifer (F1) of the HT and SH well (Figures 2c and 4a), respectively. Because the CSAP has experienced marine transgression, the elevated Cl concentration can probably be attributed to paleo-seawater in the sediment pore. This is evidenced by the enrichment of Na^+ and

Cl^- contents. Moreover, most major components, such as Ca^{2+}, Mg^{2+}, K^+, and SO_4^{2-}, have higher concentrations than other aquifers (Figures S1 and S2), particularly SO_4^{2-}, which is commonly found in seawater. Groundwater in HT-F1 demonstrates a high solute Sr level of 3.814 µM and a lower $^{87}Sr/^{86}Sr$ ratio (Figure 8) than most BGT groundwater, suggesting that paleo-seawater contributes to the elevated levels of major components. However, The Sr concentration in SH-F1 is only slightly higher than those in other groundwater samples from this region, and $^{87}Sr/^{86}Sr$ ratio agrees with the range of most samples, indicating that the influence of paleo-seawater is minimal (Figure 9). We observe that the hydrogeological setting of the HT and SH indicates that the first aquifer is very thin, likely resulting in poor lateral connection, which allows the retention of ancient seawater signals (Figure 2). In contrast, the deeper aquifer is thicker and may have better lateral connection, causing the absence of the ancient seawater signal (Figure 2).

5.5. Carbonate Weathering Influence on Proximal Fan Groundwater

According to the TDS vs. Cl^- plot of the proximal fan, we may intuitively conclude that paleo-seawater largely influenced the groundwater since it is evident that all major components show more enriched in groundwater than stream water, similar to the characteristic of paleo-seawater intrusion (Figure 6a). However, while the concentration of Na^+, Sr^{2+}, K^+, and SO_4^{2-} in the groundwater of the proximal fan are similar to those of the CSR's mainstream, only Ca^{2+}, Mg^{2+}, and HCO_3^- increased in groundwater (Figures 6b and S3), suggesting other mechanisms contribute to the elevated Ca^{2+}, Mg^{2+}, and HCO_3^- concentration. Moreover, the hydrogeological setting at the apex of CSAP is mainly composed of a highly permeable gravel layer, making it seem difficult to retain paleo-seawater signals (B-B' profile in Figure 2b). The high influx of river water into this area provides a large amount of sulfuric acid, which may accelerate the weathering of carbonate fraction in parent rocks, thereby increasing the concentrations of Ca^{2+}, Mg^{2+}, and HCO_3^- in groundwater. The Ca^{2+}+Mg^{2+} vs. HCO_3^- content plot show a strong correlation (R^2 = 0.84; Figure 10), indicating that carbonate weathering plays a vital role in controlling the water chemistry of groundwater in the proximal fan. Previous studies have indicated that water involved in carbonate weathering typically exhibits low $^{87}Sr/^{86}Sr$ ratios [14,46]. The study of Su et al. [46] performed sequential extraction on CSR's sediments, revealing an $^{87}Sr/^{86}Sr$ value of 0.712732 for the carbonate fraction, suggesting that carbonate weathering may be a factor influencing the $^{87}Sr/^{86}Sr$ ratios in this region. Although the watershed lacks pure carbonate deposits, rocks in the area have been found to contain dispersed carbonate minerals, with weight percentages ranging from 0.19% to 25.64% [31]. However, other aquifers in the proximal fan also indicate high Ca and Mg contents but their $^{87}Sr/^{86}Sr$ ratios do not decline (Figure 7 and Figure S3), implying that carbonate dissolution may not be the dominant Sr source of groundwater.

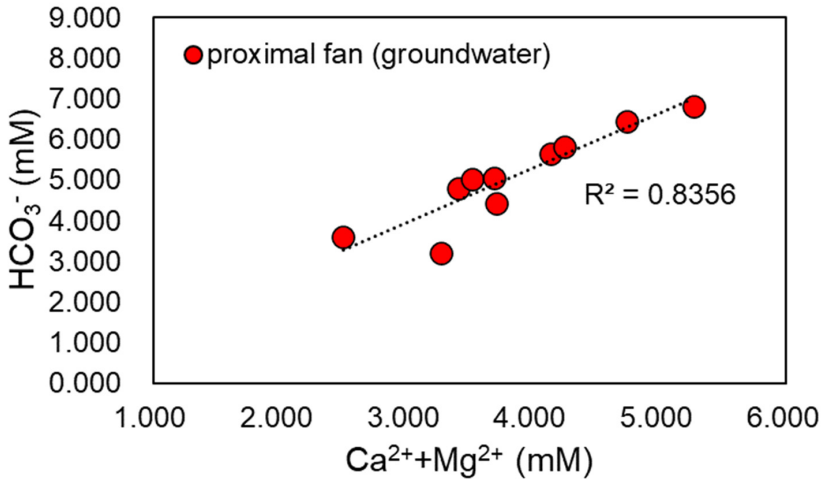

Figure 10. Ca^{2+} and Mg^{2+} vs. HCO_3^- content for the groundwater collected from proximal fan area.

6. Conclusions

In this article, we present the major ion composition, solute Sr concentrations, and $^{87}Sr/^{86}Sr$ ratios of groundwater and stream water from CSR. These parameters are tested as proxies to identify water sources and trace groundwater recharge. The Piper diagram shows that most groundwater samples belong to the freshwater Ca-HCO_3 type, consistent with the TDS classification.

TDS and major ion compositions indicate that groundwater near the BGT and DLH areas has TDS values within the range of stream water and rainwater, except for HT-F1 and SH-F1. This suggests that stream water and rainwater are the major inputs of groundwater. However, several aquifers exhibit Na^+ and Cl^- enrichment compared to stream water and rainwater. These findings are attributed to freshwater flushing marine deposits, due to the lack of evidence for anthropogenic inputs and evaporite deposits. Aquifers showing only Na^+ and Cl^- enrichment are assumed to be influenced by the dissolution of paleo-sea salt, while those with other elevated major ion concentrations are linked to mixing with paleo-seawater from sedimentary porewater in thick, poor-lateral-connection aquifers like HT-F1. The $^{87}Sr/^{86}Sr$ ratios and solute Sr levels support this assumption, as aquifers exposed to paleo-seawater demonstrate higher solute Sr concentrations and lower $^{87}Sr/^{86}Sr$ values compared to other freshwater aquifers. Groundwater in the proximal fan is affected by intensive weathering processes, resulting in high TDS values, which limit the use of TDS as a recharge tracer.

Solute Sr concentrations and $^{87}Sr/^{86}Sr$ ratios clearly indicate that groundwater in the proximal fan is primarily recharged by CSR's mainstream. In the BGT region, groundwater is dominantly replenished by the mainstream, with a small contribution from rainwater, reflected in the dilution of major ion concentrations and decreasing $^{87}Sr/^{86}Sr$ ratios. Sr isotopic composition indicates that groundwater near DLH is mainly recharged by CSR's tributaries, with minor contributions from rainwater and the mainstream.

Overall, TDS and major ion components are limited as recharge tracers due to the influence of paleo-sea salt dissolution and weathering processes. Furthermore, the CSR mainstream and tributaries exhibit only slight variations in major ion compositions and TDS values, limiting their use as tracers. In contrast, Sr isotopic compositions and solute Sr concentrations clearly distinguish the contributions of rainwater, mainstream, and tributaries in these recharge areas. Combining water chemistry data provides a better understanding of groundwater sources and the chemical processes influencing groundwater quality.

Supplementary Materials: The following supporting information can be downloaded at: https://www.mdpi.com/article/10.3390/w16152151/s1.

Author Contributions: Conceptualization, H.-W.H.; methodology, S.-T.H. and R.-M.W.; validation, H.-W.H. and C.-F.Y.; investigation, S.-T.H., R.-M.W. and W.-F.C.; writing—original draft preparation, H.-W.H.; writing—review and editing, S.-T.H., R.-M.W., C.-H.C. and C.-F.Y.; visualization, H.-W.H.; supervision, C.-F.Y. All authors have read and agreed to the published version of the manuscript.

Funding: This research was funded by NSTC, grant number 112-2116-M-006-008- to C.Y. and the APC was funded by 112-2116-M-006-008-.

Data Availability Statement: Date are contained within the article.

Acknowledgments: The authors acknowledge Taiwan Sugar Xinying Sugar Factory Groundwater Development and Conservation Center for providing the groundwater samples used in this study. We thank the two reviewers and the Editor provide us with constructive comments/suggestions in the earlier draft, which have improved this paper significantly.

Conflicts of Interest: The authors declare no conflicts of interest.

References

1. Taylor, R.G.; Scanlon, B.; Döll, P.; Rodell, M.; Van Beek, R.; Wada, Y.; Longuevergne, L.; Leblanc, M.; Famiglietti, J.S.; Edmunds, M.; et al. Ground water and climate change. *Nat. Clim. Chang.* **2013**, *3*, 322–329. [CrossRef]

2. Barthel, R.; Stangefelt, M.; Giese, M.; Nygren, M.; Seftigen, K.; Chen, D. Current understanding of groundwater recharge and groundwater drought in Sweden compared to countries with similar geology and climate. *Geogr. Ann. Ser. A Phys. Geogr.* **2021**, *103*, 323–345. [CrossRef]
3. De Vries, J.J.; Simmers, I. Groundwater recharge: An overview of processes and challenges. *Hydrogeol. J.* **2002**, *10*, 5–17. [CrossRef]
4. Earman, S.; Dettinger, M. Potential impacts of climate change on groundwater resources–a global review. *J. Water Clim. Chang.* **2011**, *2*, 213–229. [CrossRef]
5. Green, T.R.; Taniguchi, M.; Kooi, H.; Gurdak, J.J.; Allen, D.M.; Hiscock, K.M.; Treidel, H.; Aureli, A. Beneath the surface of global change: Impacts of climate change on groundwater. *J. Hydrol.* **2011**, *405*, 532–560. [CrossRef]
6. Meixner, T.; Manning, A.H.; Stonestrom, D.A.; Allen, D.M.; Ajami, H.; Blasch, K.W.; Brookfield, A.E.; Castro, C.L.; Clark, J.F.; Gochis, D.J.; et al. Implications of projected climate change for groundwater recharge in the western United States. *J. Hydrol.* **2016**, *534*, 124–138. [CrossRef]
7. Ngo TM, L.; Wang, S.J.; Chen, P.Y. Assessment of future climate change impacts on groundwater recharge using hydrological modeling in the Choushui River Alluvial Fan, Taiwan. *Water* **2024**, *16*, 419. [CrossRef]
8. Capo, R.C.; Stewart, B.W.; Chadwick, O.A. Strontium isotopes as tracers of ecosystem processes: Theory and methods. *Geoderma* **1998**, *82*, 197–225. [CrossRef]
9. Faure, G. *Principles of Isotope Geology*, 2nd ed.; Wiley: New York, NY, USA, 1986; p. 539.
10. Barbieri, M.; Boschetti, T.; Petitta, M.; Tallini, M. Stable isotope (^{2}H, ^{18}O and $^{87}Sr/^{86}Sr$) and hydrochemistry monitoring for groundwater hydrodynamics analysis in a karst aquifer (Gran Sasso, Central Italy). *Appl. Geochem.* **2005**, *20*, 2063–2081. [CrossRef]
11. Semhi, K.; Abdalla, O.; Al Abri, R.; Al Hosni, T.; Clark, I.D. Strontium isotopes as a tool for estimation of groundwater recharge and aquifer connectivity. *Groundw. Sustain. Dev.* **2017**, *4*, 1–11. [CrossRef]
12. Christensen, J.N.; Dafflon, B.; Shiel, A.E.; Tokunaga, T.K.; Wan, J.; Faybishenko, B.; Dong, W.; Williams, K.H.; Hobson, C.; Brown, S.T.; et al. Using strontium isotopes to evaluate the spatial variation of groundwater recharge. *Sci. Total Environ.* **2018**, *637*, 672–685. [CrossRef]
13. Gosselin, D.C.; Harvey, F.E.; Frost, C.; Stotler, R.; Macfarlane, P.A. Strontium isotope geochemistry of groundwater in the central part of the Dakota (Great Plains) aquifer, USA. *Appl. Geochem.* **2004**, *19*, 359–377. [CrossRef]
14. Bakari, S.S.; Aagaard, P.; Vogt, R.D.; Ruden, F.; Johansen, I.; Vuai, S.A. Strontium isotopes as tracers for quantifying mixing of groundwater in the alluvial plain of a coastal watershed, south–eastern Tanzania. *J. Geochem. Explor.* **2013**, *130*, 1–14. [CrossRef]
15. Meredith, K.; Moriguti, T.; Tomascak, P.; Hollins, S.; Nakamura, E. The lithium, boron and strontium isotopic systematics of groundwaters from an arid aquifer system: Implications for recharge and weathering processes. *Geochim. Cosmochim. Acta* **2013**, *112*, 20–31. [CrossRef]
16. Zhang, C.; Li, X.; Wang, Z.; Hou, X.; Ma, J.; Gao, M.; Bai, Z.; Fu, C.; Gui, C.; Zuo, X. Combining stable isotope (^{2}H, ^{18}O, and $^{87}Sr/^{86}Sr$) and hydrochemistry to understand hydrogeochemical processes in karst groundwater system, Xin'an, northern China. *Environ. Earth Sci.* **2023**, *82*, 224. [CrossRef]
17. Central Geological Survey. Project of Groundwater Monitoring Network in Taiwan During First-Stage-Research Report of Chou-Shui River Alluvial Fan. *Water Resour. Bur. Rep.* **1999**, *130*, 100.
18. Central Geological Survey. *Designation of Choshuichi Alluvial Fan Groundwater Recharge Geologically Sensitive Area*; Ministry of Economic Affairs: Taipei, Taiwan, 2014; p. 105. (In Chinese)
19. Central Geological Survey. *Investigation of Hydrogeological Characteristics of Aquifers and Groundwater Resource Assessment (1/5)*; Ministry of Economic Affairs: Taipei, Taiwan, 2022; p. 108. (In Chinese)
20. Hsu, C.H.; Han, S.T.; Kao, Y.H.; Liu, C.W. Redox characteristics and zonation of arsenic–affected multi–layers aquifers in the Choushui River alluvial fan, Taiwan. *J. Hydrol.* **2010**, *391*, 351–366. [CrossRef]
21. Chung, C.H.; You, C.F.; Chu, H.Y. Weathering sources in the Gaoping (Kaoping) river catchments, southwestern Taiwan: Insights from major elements, Sr isotopes, and rare earth elements. *J. Mar. Syst.* **2009**, *76*, 433–443. [CrossRef]
22. Freeze, R.A.; Cherry, J.A. *Groundwater*; Prentice-Hall: Englewood Cliffs, NJ, USA, 1979; p. 604.
23. Chang, T.; Wang, K.; Wang, S.; Hsu, C.; Hsu, C. Evaluation of the Groundwater and Irrigation Quality in the Zhuoshui River Alluvial Fan between Wet and Dry Seasons. *Water* **2022**, *14*, 1494. [CrossRef]
24. Appelo CA, J. Cation and proton exchange, pH variations, and carbonate reactions in a freshening aquifer. *Water Resour. Res.* **1994**, *30*, 2793–2805. [CrossRef]
25. Lu, H.Y.; Peng, T.R.; Liou, T.S. Identification of the origin of salinization in groundwater using multivariate statistical analysis and geochemical modeling: A case study of Kaohsiung, Southwest Taiwan. *Environ. Geol.* **2008**, *55*, 339–352. [CrossRef]
26. Islam, M.S.; Mostafa, M.G. Evaluation of hydrogeochemical processes in groundwater using geochemical and geostatistical approaches in the upper Bengal basin. *Geofluids* **2022**, *2022*, 9591717. [CrossRef]
27. Chae, G.T.; Yun, S.T.; Kim, K.; Mayer, B. Hydrogeochemistry of sodium–bicarbonate type bedrock groundwater in the Pocheon spa area, South Korea: Water–rock interaction and hydrologic mixing. *J. Hydrol.* **2006**, *321*, 326–343. [CrossRef]
28. Central Geological Survey. *Central Geological Survey Explanatory Text of the Geologic Map of Yulin (1:50,000)*; Ministry of Economic Affairs: Taipei, Taiwan, 2004; p. 4.
29. Calmels, D.; Galy, A.; Hovius, N.; Bickle, M.; West, A.J.; Chen, M.C.; Chapman, H. Contribution of deep groundwater to the weathering budget in a rapidly eroding mountain belt, Taiwan. *Earth Planet. Sci. Lett.* **2011**, *303*, 48–58. [CrossRef]

30. Das, A.; Chung, C.H.; You, C.F. Disproportionately high rates of sulfide oxidation from mountainous river basins of Taiwan orogeny: Sulfur isotope evidence. *Geophys. Res. Lett.* **2012**, *39*, L12404. [CrossRef]
31. Meyer, K.J.; Carey, A.E.; You, C.F. Typhoon impacts on chemical weathering source provenance of a High Standing Island watershed, Taiwan. *Geochim. Cosmochim. Acta* **2017**, *215*, 404–420. [CrossRef]
32. Barth, J.A.; Stichler, W.; Bergemann, M.; Reincke, H. Can conductivity and stable isotope tracers determine water sources during flooding? An example from the Elbe River in 2002. *Int. J. River Basin Manag.* **2006**, *4*, 77–83. [CrossRef]
33. Maurya, A.S.; Shah, M.; Deshpande, R.D.; Bhardwaj, R.M.; Prasad, A.; Gupta, S.K. Hydrograph separation and precipitation source identification using stable water isotopes and conductivity: River Ganga at Himalayan foothills. *Hydrol. Process.* **2011**, *25*, 1521–1530. [CrossRef]
34. Liu, Y.; Yamanaka, T. Tracing groundwater recharge sources in a mountain–plain transitional area using stable isotopes and hydrochemistry. *J. Hydrol.* **2012**, *464*, 116–126. [CrossRef]
35. Peng, T.R.; Lu, W.C.; Chen, K.Y.; Zhan, W.J.; Liu, T.K. Groundwater–recharge connectivity between a hills–and–plains' area of western Taiwan using water isotopes and electrical conductivity. *J. Hydrol.* **2014**, *517*, 226–235. [CrossRef]
36. Appelo CA, J.; Postma, D. *Geochemistry, Groundwater and Pollution*; CRC Press: London, UK, 2005.
37. Subyani, A.M. Use of chloride–mass balance and environmental isotopes for evaluation of groundwater recharge in the alluvial aquifer, Wadi Tharad, western Saudi Arabia. *Environ. Geol.* **2004**, *46*, 741–749. [CrossRef]
38. Cox, M.H.; Su, G.W.; Constantz, J. Heat, chloride, and specific conductance as ground water tracers near streams. *Groundwater* **2007**, *45*, 187–195. [CrossRef] [PubMed]
39. Manna, F.; Cherry, J.A.; McWhorter, D.B.; Parker, B.L. Groundwater recharge assessment in an upland sandstone aquifer of southern California. *J. Hydrol.* **2016**, *541*, 787–799. [CrossRef]
40. Aliewi, A.; Bhandary, H.; Sabarathinam, C.; Al-Qallaf, H. A new modified chloride mass balance approach based on aquifer hydraulic properties and other sources of chloride to assess rainfall recharge in brackish aquifers. *Hydrol. Process.* **2022**, *36*, e14513. [CrossRef]
41. Li, Y.H.; Chen, C.T.; Hung, J.J. Aquatic chemistry of lakes and reservoirs in Taiwan. *TAO* **1997**, *8*, 405. [CrossRef]
42. Cheng, M.C.; You, C.F.; Lin, F.J.; Chung, C.H.; Huang, K.F. Seasonal variation in long–range transported dust to a subtropical islet offshore northern Taiwan: Chemical composition and Sr isotopic evidence in rainwater. *Atmos. Environ.* **2010**, *44*, 3386–3393. [CrossRef]
43. Li, C.; Gao, X.; Liu, Y.; Wang, Y. Impact of anthropogenic activities on the enrichment of fluoride and salinity in groundwater in the Yuncheng Basin constrained by Cl/Br ratio, $\delta^{18}O$, $\delta^{2}H$, $\delta^{13}C$ and $\delta^{7}Li$ isotopes. *J. Hydrol.* **2019**, *579*, 124211. [CrossRef]
44. Xu, Z.; Liu, C.Q. Chemical weathering in the upper reaches of Xijiang River draining the Yunnan–Guizhou Plateau, Southwest China. *Chem. Geol.* **2007**, *239*, 83–95. [CrossRef]
45. Liu, C.Q.; Lang, Y.C.; Satake, H.; Wu, J.; Li, S.L. Identification of anthropogenic and natural inputs of sulfate and chloride into the karstic ground water of Guiyang, SW China: Combined $\delta^{37}Cl$ and $\delta^{34}S$ approach. *Environ. Sci. Technol.* **2008**, *42*, 5421–5427. [CrossRef]
46. Su, N.; Yang, S.; Deng, K.; Chang, Y.P.; Xu, J.; Wu, Z. Radiogenic and stable Sr isotopes constrain weathering processes in rapidly eroding Taiwan catchments. *Earth Planet. Sci. Lett.* **2021**, *576*, 117235. [CrossRef]

Disclaimer/Publisher's Note: The statements, opinions and data contained in all publications are solely those of the individual author(s) and contributor(s) and not of MDPI and/or the editor(s). MDPI and/or the editor(s) disclaim responsibility for any injury to people or property resulting from any ideas, methods, instructions or products referred to in the content.